EJN fens EUROPEAN JOURNAL OF NEUROSCIENCE

European Journal of Neuroscience, Vol. 35, pp. 673–681, 2012 doi:10.1111/j.1460-9568.2012.07995.x

MOLECULAR AND DEVELOPMENTAL NEUROSCIENCE

Synchronized spike waves in immature dentate gyrus networks

Megumi Seki,* Chiaki Kobayashi,* Naoya Takahashi, Norio Matsuki and Yuji Ikegaya
Laboratory of Chemical Pharmacology, Graduate School of Pharmaceutical Sciences, The University of Tokyo, Bunkyo-ku, Tokyo, Japan

Keywords: calcium, development, hippocampus, learning and memory, mouse, stress

Abstract

At early developmental stages, immature neuronal networks of the neocortex and hippocampus spontaneously exhibit synchronously oscillating activities, which are believed to play roles in normal circuit maturation. The tissue development of the dentate gyrus (DG) in the hippocampal formation is exceptionally late compared with other brain regions and persists until postnatal periods. Using patch-clamp recording and functional multineuron calcium imaging, we found that the DG networks of postnatal day (P)3–7 mice spontaneously generated traveling waves of action potentials, which were initiated at the upper blade of the granule cell layer and propagated to the lower blade. The propagation was dependent on glutamatergic and electrical synapses, but not on GABAergic receptor activity. Remarkably, the DG waves were almost completely abolished in offspring born to female rats exposed to restraint stress during pregnancy. In the prenatally stressed offspring, DG granule cell dendrites developed normally until P3 and showed atrophy by P9. Thus, the DG waves may be required for the maturation of DG granule cells.

Introduction

Immature neuronal networks exhibit large-scale rhythmic activity. These early network oscillations prevail in various regions of the developing brain, including the neocortex (Yuste *et al.*, 1992; Garaschuk *et al.*, 2000), hippocampus (Ben-Ari *et al.*, 1989), and cerebellum (Watt *et al.*, 2009). These oscillations are accompanied by intracellular calcium elevations and may regulate neuronal differentiation, neurite elongation, synaptogenesis, and network formation (Spitzer, 2006; Blankenship & Feller, 2010), although their functional significance has not been strictly defined.

In the rodent hippocampal formation, the dentate gyrus (DG) primarily develops during the first postnatal week (Altman & Bayer, 1990). Although neurogenesis of DG granule cells persists into adulthood, the granule cells formed during this neonatal period predominate in the adult DG (Muramatsu *et al.*, 2007). Therefore, the considerable structural reorganization in postnatal DG networks provides a useful experimental model to examine the early development of brain networks and the long-term consequences of the development process. In the present study, we report that the developing DG exhibits a novel form of early network waves.

Stress has long-term sequelae; for instance, the risk of major depressive disorder increases in adults who suffered from stress early in life. In animal models (Hosseini-Sharifabad & Hadinedoushan, 2007; Tamura *et al.*, 2011), offspring born to female rats exposed to restraint stress during pregnancy exhibit poorly arborized dendritic trees of granule cells in the DG, an area of the brain whose malformation has been implicated in depression and cognitive deficit. However, it is unknown when and how this dendritic atrophy appears during development. We found that, in mice exposed to prenatal stress, granule cell dendrites developed normally until postnatal day (P)3 and showed atrophy by P9. Remarkably, the DG waves were almost completely abolished in P3 mice that had been exposed to prenatal stress. Thus, the DG network waves may underlie the maturation of DG granule cells.

Materials and methods

Animal experiment ethics

All experiments were performed with the approval of the animal experiment ethics committee at the University of Tokyo (approval number 19–35) and in accordance with the University of Tokyo guidelines for the care and use of laboratory animals.

Slice preparations

The P1–13 ICR mice of either sex (SLC, Shizuoka, Japan) were anesthetized with ether and decapitated. The brain was immersed in ice-cold modified artificial cerebrospinal fluid (aCSF) consisting of (in mM) – 27 $NaHCO_3$, 1.4 NaH_2PO_4, 2.5 KCl, 0.5 ascorbic acid, 7.0 $MgSO_4$, 1.0 $CaCl_2$, and 222 sucrose, bubbled with 95% O_2 and 5% CO_2. Entorhino-hippocampal slices were cut at a thickness of 400 μm

Correspondence: Yuji Ikegaya, as above.
E-mail: ikegaya@mol.f.u-tokyo.ac.jp

*M.S. and C.K. contributed equally to this work.

Received 12 September 2011, revised 14 November 2011, accepted 11 December 2011

using a vibratome (VT1200S; Leica, Heidelberg, Germany). Unless otherwise specified, the slices were made in the horizontal direction. They were maintained for more than 30 min at room temperature (23–25 °C) in normal aCSF consisting of (in mM) – 127 NaCl, 26 $NaHCO_3$, 1.6 KCl, 1.24 KH_2PO_4, 1.3 $MgSO_4$, 2.4 $CaCl_2$, and 10 glucose. In some experiments, a small incision was manually made in the slices. After a slice was placed in a recording chamber, the molecular layer or the hilus was carefully incised at the DG crest in the direction perpendicular to the granule cell layer using a surgical microknife under transmitted-light microscopic control.

Calcium imaging

Slices were incubated for 20–40 min at room temperature with 0.0005% Oregon Green 488 1,2-bis(o-aminophenoxy)ethane-N,N,N′,N′-tetraacetic acid-1 acetoxymethyl ester (Invitrogen, Gaithersburg, MD, USA), 0.01% Pluronic F-127 (Invitrogen), and 0.005% Cremophor EL (Sigma-Aldrich, St Louis, MO, USA), and were allowed to recover in aCSF for 60 min. The slices were transferred to a recording chamber perfused with aCSF at a rate of 1.5–2.0 mL/min. The emergence of the traveling waves did not significantly differ between 23–25 °C and 35–37 °C (Supporting Information Fig. S1). Therefore, unless otherwise specified, data were acquired at 23–25 °C, which enabled optical imaging for a longer time. Calcium activity was imaged from the DG. Images (16-bit intensity, 256×256 or 512×512 pixels, 410×410 μm^2) were captured at 10–50 frames/s with a Nipkow-disk confocal unit (CSU-X1; Yokogawa Electric, Tokyo, Japan), a cooled charge-coupled device camera (iXon DU897; Andor Technology, Belfast, UK), an upright microscope (Axio Examiner D1; Carl Zeiss, Oberkochen, Germany) with a water-immersion objective (20 ×, 1.0 numerical aperture; Carl Zeiss), and image acquisition software (SOLIS, Andor Technology). Fluorophores were excited at 488 nm with an argon–krypton laser (10–15 mW, 641-YB-A01; Melles Griot, Carlsbad, CA, USA) and visualized using a 507-nm long-pass emission filter. Data analysis was performed with custom-made software written in Microsoft Visual Basic and Matlab. Neurons were numbered along the longitudinal axis of the granule cell layer in a direction from the upper blade to the lower blade. Fluorescence changes in the soma of each cell were measured as $(F_t - F_0)/F_0$, where F_t is the fluorescence intensity at any time point and F_0 is the average baseline across 10 s before and after time t. Neurons were discriminated from other cell types, such as glia, based on the kinetics of their calcium dynamics (Sasaki *et al.*, 2007). The onsets of calcium signals were determined by thresholding 4 × SDs of the baseline. The events of all neurons recorded in a single movie (typically 100–250 neurons) were combined into a raster plot. Any synchronized activity that recruited more than 40% of the total monitored cells at the same time was defined as an early network wave-relevant event. All other calcium activities were regarded as wave-irrelevant events, termed 'sporadic' activity. The onset timings of individual calcium events were approximated to a single linear function using the least-squares method, and the best-fit slope was used to calculate the velocity of the wave propagation.

Electrophysiology

Granule cells were visually identified using infrared differential interference contrast microscopy. For loose cell-attached recordings, borosilicate glass pipettes (7–9 MΩ) were filled with aCSF (Sasaki *et al.*, 2011). For whole-cell recordings, borosilicate glass pipettes (7–9 MΩ) were filled with a solution consisting of 120 mM K-gluconate, 20 mM KCl, 5 mM NaCl, 4 mM $MgCl_2$, 10 mM HEPES, 10 mM phosphocreatine, 4 mM MgATP, 0.3 mM NaGTP, and 0.1 mM EGTA. Data were obtained using a MultiClamp 700B amplifier and a Digidata 1440A digitizer controlled by pCLAMP 10 software (Molecular Devices, Union City, CA, USA). Signals were low-pass filtered at 2 kHz and digitized at 20 kHz.

Pharmacology

Tetrodotoxin (1 μM), picrotoxin (50 μM), D,L-2-amino-5-phosphonopentanoic acid (50 μM), carbenoxolone (100 μM), 6-cyano-7-nitroquinoxaline-2,3-dione (10 μM), and 18-β-glycyrrhetinic acid (100 μM) were purchased from Sigma-Aldrich. The drug solution was prepared immediately before use and perfused into the recording chamber.

Prenatal stress

Pregnant female ICR mice were housed individually after embryonic day 13–19 and were subjected to a repeated restraint stress procedure according to Lemaire *et al.* (2000). A pregnant mouse was forced to stay in a transparent cylindrical cage (φ 3 cm) that was illuminated at 2000 lux. A single session lasted for 45 min and was repeated three times at intervals of 2.5–5 h within 1 day. This procedure was applied every day from embryonic day 13 until delivery, i.e. embryonic day 19. Each session was conducted during the light phase, but the start time was not fixed to avoid prediction or habituation to the restraint stress. Control mice were kept in home cages.

Immunohistochemistry

After experiments, slices were postfixed with 4% paraformaldehyde at 4 °C for 24 h. The fixed slices were rinsed three times with 0.1 M phosphate buffer and incubated overnight at 4 °C in 0.1% TritonX-100 and 5% goat serum/phosphate buffer. They were incubated with primary antibodies (mouse anti-neuronal nuclear antigen, 1 : 1000; Chemicon, Temecula, CA, USA; rabbit anti-Prox1, 1 : 5000; Chemicon) and then with Alexa Fluor 488- or 594-conjugated secondary antibodies (1 : 1000; Invitrogen) at room temperature for 2 h. The samples were observed with a Bio-Rad MRC-1024 confocal system. *Z*-series images were collected at 1–2-μm steps and 11–21 *Z*-sections (20-μm thickness) were stacked.

Sholl analysis

For electroporation, patch-clamp pipettes were filled with 400 μM Alexa Fluor 568 and 1% biocytin in double-distilled water and attached to the cell body of a DG granule cell. A single 10-ms pulse of 10 V or multiple 500-μs pulses of 6–10 V (50 trains at 500 Hz) were delivered through the pipette (Takahashi *et al.*, 2012). After an overnight fixation with 4% paraformaldehyde and 0.03% glutaraldehyde, the slices were incubated at room temperature with 0.3% Triton-X 100 for 1 h followed by Alexa Fluor 488-conjugated streptavidin (1 : 500, S32354; Invitrogen) for 2 days. The neurons were imaged using a CSU-Frontier confocal system (Yokogawa Electric). Their morphologies were reconstructed using a camera lucida and quantified by counting the number of dendrite intersections with concentric circles centered at the centroid of the cell body. The radius was increased at a step of 5 μm. Granule cells located in the outer layer of the DG upper blade were selected for analysis because the cell

maturation may differ depending on the cell location (Altman & Bayer, 1990). Data were analyzed in a double-blind manner.

Data representation

Data are reported as the means ± SEM.

Results

Synchronized activity of the dentate gyrus occurred only during early development

Acute slices of the immature hippocampal formation prepared from P1 to P13 mice were loaded with 0.0005% Oregon Green 488 1,2-bis (o-aminophenoxy)ethane-N,N,N′,N′-tetraacetic acid-1 acetoxymethyl ester, and the activity of DG neurons was monitored using functional multineuron calcium imaging (Fig. 1A and B). In all the slices tested, DG neurons spontaneously exhibited transient calcium elevations. The activity pattern is presented in a raster plot in which cells were assigned serial numbers along the longitudinal axis of the DG granule cell layer; higher numbers were given to cells closer to the end of the lower blade of the granule cell layer. The raster plots revealed that the spatiotemporal patterns of DG activity varied depending on the ages of the mice (Fig. 1C). The distributions for the event frequency of each cell are shown in Fig. 1D. The majority of neuronal activity was asynchronous during P1–P2 and P7–P13, but, among these sporadic calcium events, synchronized waves intermittently occurred during P3–P7. These synchronous events were traveling waves that gradually propagated from the upper blade to the lower blade and recruited more than 40% of DG neurons (Fig. 1C, middle inset). The waves were stereotypic and did not propagate in the opposite direction. The propagation velocity was 482 ± 25 μm/s (n = 632 events from 33 slices). The waves appeared most frequently on P3, when the frequency reached 1.6 ± 0.3 waves/min. Thereafter, the waves became infrequent and eventually disappeared until P9 (Fig. 1E; $F_{1,7} = 30.3$, $P = 3.7 \times 10^{-12}$, one-way ANOVA; $P < 0.05$, P3 vs. P1, P2, P5, P7, P9, P11, and P13, Bonferroni/Dunn test), but the level of sporadic activity remained constant or slightly increased during P1–P9 (Fig. 1F; $F_{1,7} = 5.82$, $P = 0.0002$, one-way ANOVA; $P < 0.05$, P1, P2, P3 vs. P9, Bonferroni/Dunn test). The waves were observed not only in horizontal brain slices, but also in coronal and sagittal slices (Fig. 2), which suggests that the waves prevail in the entire hippocampal formation, including the dorsal and ventral part.

Dentate gyrus wave propagation was structured by neuronal networks

Loose cell-attached recordings from DG granule cells revealed that transient calcium elevations reflected action potentials (Fig. 1B). Consistent with this observation, the traveling waves were blocked by bath application of tetrodotoxin, a voltage-sensitive sodium channel inhibitor (Fig. 3). These waves were also blocked by the non-*N*-methyl-D-aspartate receptor antagonist 6-cyano-7-nitroquinoxaline-2,3-dione and the *N*-methyl-D-aspartate receptor antagonist D,L-2-amino-5-phosphonopentanoic acid but not by the $GABA_A$ receptor antagonist picrotoxin (Fig. 3). The data indicate that traveling waves were mediated by ionotropic glutamatergic synaptic transmission. In addition, the DG waves were sensitive to the gap junction blockers carbenoxolone and 18-β-glycyrrhetic acid (Fig. 3).

To address the involvement of DG afferents, such as perforant path inputs, in the wave generation, we isolated the DG from slice preparations (Fig. 4). The DG mini-slices still generated spontaneous waves. Thus, the wave initiator is embedded in the DG networks and can operate independently of external inputs from the entorhinal cortex or Ammon's horn.

We sought to examine whether the direct stimulation of the DG triggers traveling waves. Stimulating electrodes were placed on the end of the upper or lower blade, and a train of electrical stimulation (three pulses at 100 Hz, 50-μs duration at 30 μA) was applied (Fig. 5A). The traveling waves were reliably evoked by stimulation of the upper blade but not by stimulation of the lower blade (Fig. 5A and B). The propagation velocity of the evoked waves was 452 ± 17 μm/s (n = 76 events from eight slices) and was not significantly different from that of spontaneous waves ($t_{74} = 0.30$, $P = 0.76$, Student's t-test). The pharmacological characteristics of the stimulus-evoked waves did not differ from those of spontaneous waves (Fig. 5C). These results suggest that the unidirectionality of wave propagation arose from the network structure and was probably biased by the synaptic direction.

To elucidate the propagation mechanisms, we made a partial surgical incision in the DG. The hilus or molecular layer was incised vertical to the granule cell layer, and the upper blade end was electrically stimulated (Fig. 5D). The evoked waves did not propagate across the incised line in slices with the hilus lesion, but the molecular layer lesion did not affect wave propagation (Fig. 5D and E). Therefore, the mossy fiber axons or basal dendrites of granule cells seem to be responsible for wave propagation.

Prenatal stress attenuated dentate gyrus wave initiation and the subsequent maturation of granule cells

Gestational stress impairs the topological complexity of dendrites of DG granule cells in offspring (Hosseini-Sharifabad & Hadinedoushan, 2007; Tamura *et al.*, 2011) and attenuates the expression of synaptophysin and synaptotagmin-1 (Afadlal *et al.*, 2010) and the density of dendritic spines in the hippocampus of the offspring (Martinez-Tellez *et al.*, 2009; Tamura *et al.*, 2011). These prenatally stressed animals show deficits in learning and memory and depression-like behavior (Aleksandrov *et al.*, 2001; Hosseini-Sharifabad & Hadinedoushan, 2007; Tamura *et al.*, 2011). However, no study to date has investigated the effect of early life stress on early network oscillations. We examined whether prenatal stress influences the generation of DG waves. Pregnant female mice were restrained for 45 min × 3 times per day during the last week of gestation, and postnatal DG waves were examined in their offspring (Fig. 6A). We did not observe waves in slices prepared from stressed P3 offspring (Fig. 6B). We traced this aberration up to P7 and found that the frequency of wave events was severely attenuated in stressed mice (Fig. 6C; $F_{1,28} = 37.7$, $P = 1.3 \times 10^{-6}$ for main effect of stress; $F_{2,28} = 1.74$, $P = 0.19$ for postnatal day × stress interaction; two-way ANOVA). The level of sporadic activity in P5 and P7 mice was also lower than in control mice (Fig. 6D; $F_{1,28} = 6.24$, $P = 0.018$ for main effect of stress; $F_{2,28} = 3.28$, $P = 0.052$ for postnatal day × stress interaction; two-way ANOVA). We next stimulated the upper blade end. Unlike spontaneous activity, stimulus-evoked waves were normal in stressed offspring, although the probability of evoking waves in stressed P7 mice was slightly lower than that in control P7 mice (Fig. 6E; $F_{1,32} = 39.5$, $P = 4.8 \times 10^{-7}$ for main effect of stress; $F_{2,32} = 53.3$, $P = 6.53 \times 10^{-11}$ for postnatal day × stress interaction; two-way ANOVA). The propagation velocity of the evoked waves in stressed mice was 455 ± 4 μm/s (n = 48 events from five P3 slices) and was not significantly different from that of spontaneous waves in control DG slices ($t_{74} = 0.01$, $P = 0.95$, Student's t-test).

We finally addressed whether the stress induced the morphological or electrophysiological aberrations in the DG. The immunoreactivity

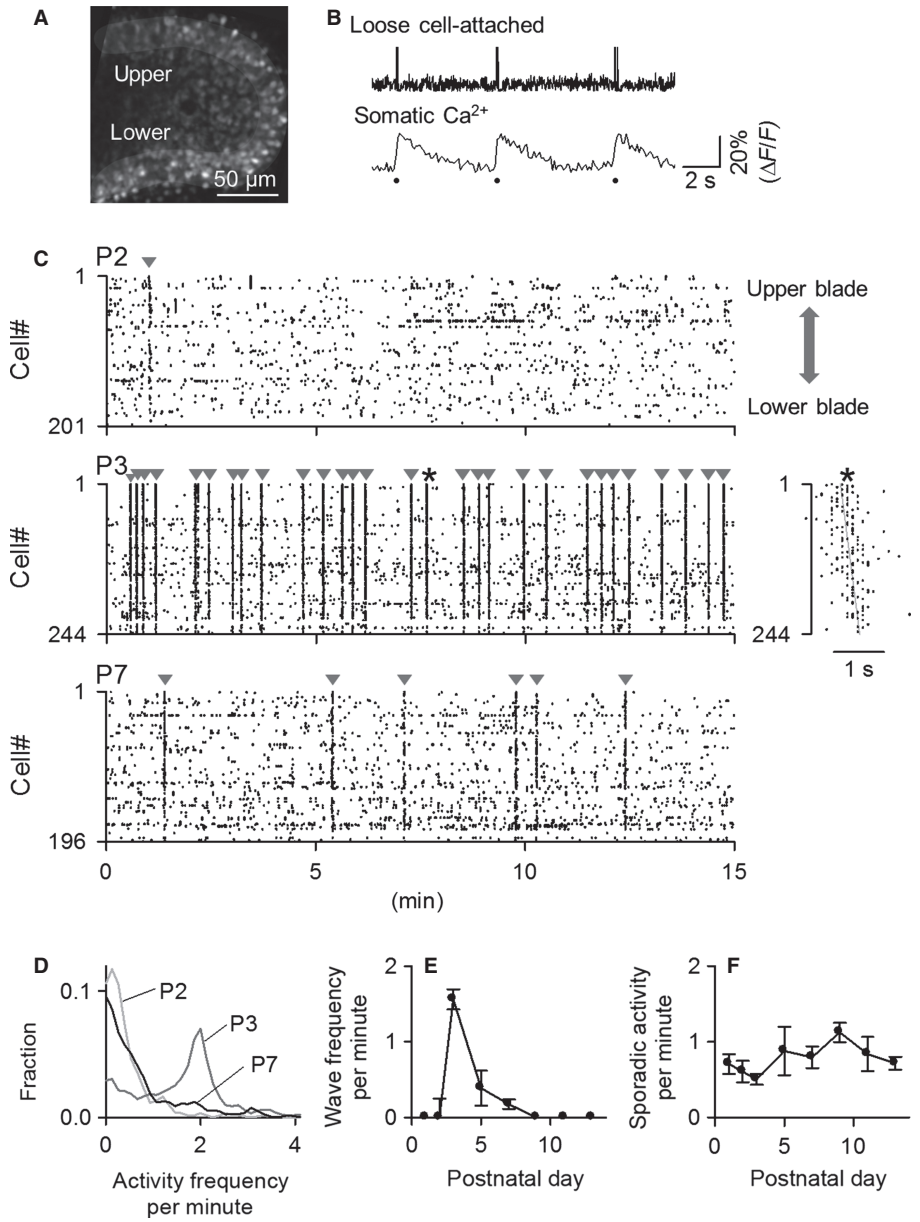

FIG. 1. Immature DG networks exhibit traveling calcium waves. (A) Confocal image of a 0.0005% Oregon Green 488 1,2-bis(o-aminophenoxy)ethane-N,N,N′,N′-tetraacetic acid-1 acetoxymethyl ester-loaded slice. (B) Simultaneous loose cell-attached recording and somatic calcium imaging from a P3 granule cell revealed that transient calcium elevations in the cell body reflected action potentials. Bottom dots denote the onset timing of calcium events. (C) Raster plots represent the spatiotemporal activity patterns in DG slices prepared from P2, P3, and P7 mice. Each dot indicates a single calcium event of the corresponding cell. Sporadic activity dominated on P2 and P7, whereas synchronous events (indicated by arrowheads) appeared frequently on P3. The asterisked event is time-expanded in the right panel. The synchronous events were waves that traveled from the upper blade to the lower blade of the DG granule cell layer. (D) Distributions of the rate of calcium events, including sporadic and wave activities, in individual cells. Developmental changes in the frequency of traveling waves (E) and sporadic activity (F). n = 4–7 slices from three to four animals for each postnatal day. Error bars represent SEMs.

for the neuron marker neuronal nuclear antigen and the DG granule cell marker Prox1 was assessed in P3 and P9 control mice and mice born to prenatally stressed females (Fig. 7A and B). Neither the apparent cell alignment nor the number of neurons differed between control and stressed pups (data not shown). The Sholl analysis of the morphology of DG granule cells revealed no impairment in the dendritic architecture in stressed P3 mice (Fig. 7C; $F_{1,374} = 0.10$, $P = 0.76$ for main effect of stress; $F_{16,374} = 0.67$, $P = 0.82$ for distance × stress interaction; two-way repeated-measures ANOVA). On P9, however, the dendritic trees were poorly arborized compared with those in control mice (Fig. 7D; $F_{1,672} = 29.2$, $P = 8.9 \times 10^{-8}$ for main effect of stress; $F_{31,672} = 0.63$, $P = 0.95$ for distance × stress interaction; two-way repeated-measures ANOVA). The total length of dendrites was 366 ± 43 μm for P3 control, 296 ± 31 μm for P3 stress, 810 ± 89 μm for P9 control, and 539 ± 90 μm for P9 stress; there was no significant difference at either age although a tendency existed between control and prenatally stressed mice. Some reports demonstrate that immature DG granule cells in the rodent bear basal dendrites (Claiborne *et al.*, 1990; Seay-Lowe & Claiborne, 1992), but we found no basal dendrites in any neuron tested. This may be due to different animal strains, which are known to have a large impact on the maturation stage of neurons.

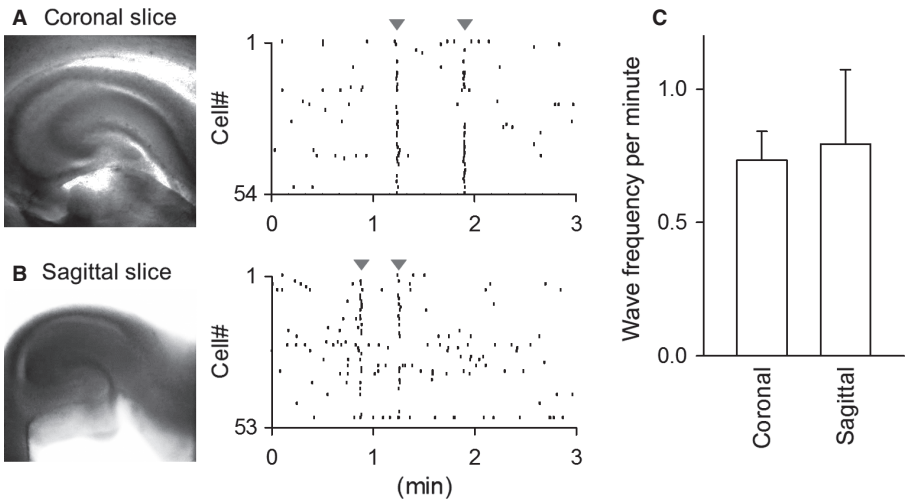

FIG. 2. DG traveling waves occur irrespective of the orientation of brain slices. Images (left) and raster plots (right) of coronal (A) and sagittal (B) P3 slices. (C) Wave frequencies in coronal and sagittal brain slices. Error bars represent SEMs of 12–14 slices from three to four animals for each group.

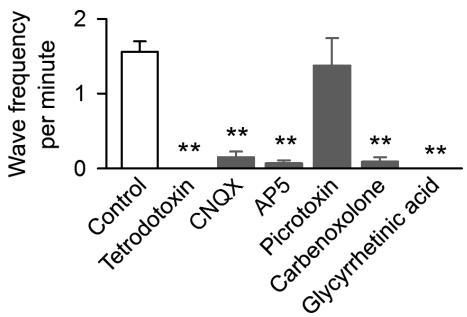

FIG. 3. DG traveling waves depend on electrical and chemical neuronal excitability. Pharmacological characterization of DG waves was conducted using P3 slices. Waves depended on glutamatergic synapses and electrical synapses, but not on GABAergic synapses. $n = 5$ slices from three to four animals each, $^{**}P < 0.01$ vs. control, Dunnett's test after one-way ANOVA. Error bars represent SEMs. AP5, D,L-2-amino-5-phosphonopentanoic acid; CNQX, 6-cyano-7-nitroquinoxaline-2,3-dione.

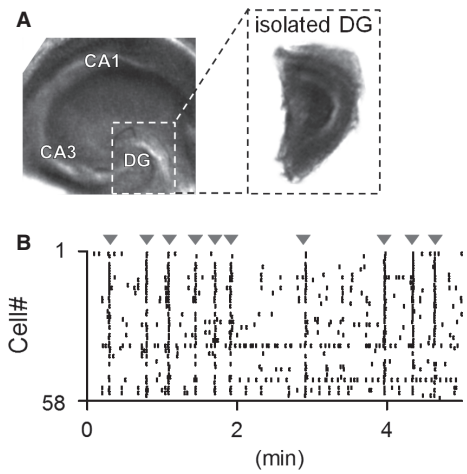

FIG. 4. Traveling waves are initiated within DG networks. (A) Mini-slices of the DG region (isolated DG) were dissected from P3 slices. (B) The mini-slices exhibited waves. Similar results were observed in all six slices from four animals tested.

For electrophysiological intrinsic properties, the membrane capacitance and resistance of stressed P3–4 mice were significantly lower and higher, respectively, than those in control mice, whereas neither resting membrane potential nor action potential threshold was affected by stress (Fig. 7E). Therefore, the aberration in the wave generation and the electrical properties preceded the dendritic atrophy.

Discussion

We demonstrated that developing DG networks generate large-scale spontaneous waves of action potentials irrespective of external inputs. The waves traveled from the upper blade to the lower blade and depended on glutamatergic and electrical synapses. The waves emerged only during a few postnatal days, but they did not appear in age-matched pups born to dams that had experienced restraint stress during pregnancy.

Dentate gyrus waves as a new form of excitability

The DG traveling waves do not resemble any type of previously known early network oscillations in the brain. A typical form of postnatal hippocampal oscillations is giant depolarizing potentials, which are mediated by the excitatory effect of $GABA_A$ receptor activation (Ben-Ari *et al.*, 1989; Leinekugel *et al.*, 1997). The DG waves, however, were insensitive to $GABA_A$ receptor antagonists. This pharmacology also differentiates the DG waves from the $GABA_A$ receptor-dependent traveling spike waves reported in the cerebellum (Watt *et al.*, 2009). Because DG waves were blocked by inhibitors of non-*N*-methyl-D-aspartate receptors, *N*-methyl-D-aspartate receptors, and gap junctions, they are also different from nicotinic acetylcholine receptor-dependent waves in the retina (McLaughlin *et al.*, 2003) or ATP-dependent waves in the cochlea (Tritsch *et al.*, 2007). Rather, the mechanism responsible for DG waves is ostensibly similar to immature neocortical oscillations (Garaschuk *et al.*, 2000). However, the propagation speed is incompatible; the velocity of neocortical waves is about 2 mm/s (Garaschuk *et al.*, 2000), whereas the velocity of DG waves was about 0.5 mm/s. Moreover, the DG waves were unidirectional even when evoked by electrical stimulation, whereas neocortical waves are bidirectional (Garaschuk *et al.*, 2000). This directional preference in the DG waves suggests that glutamatergic

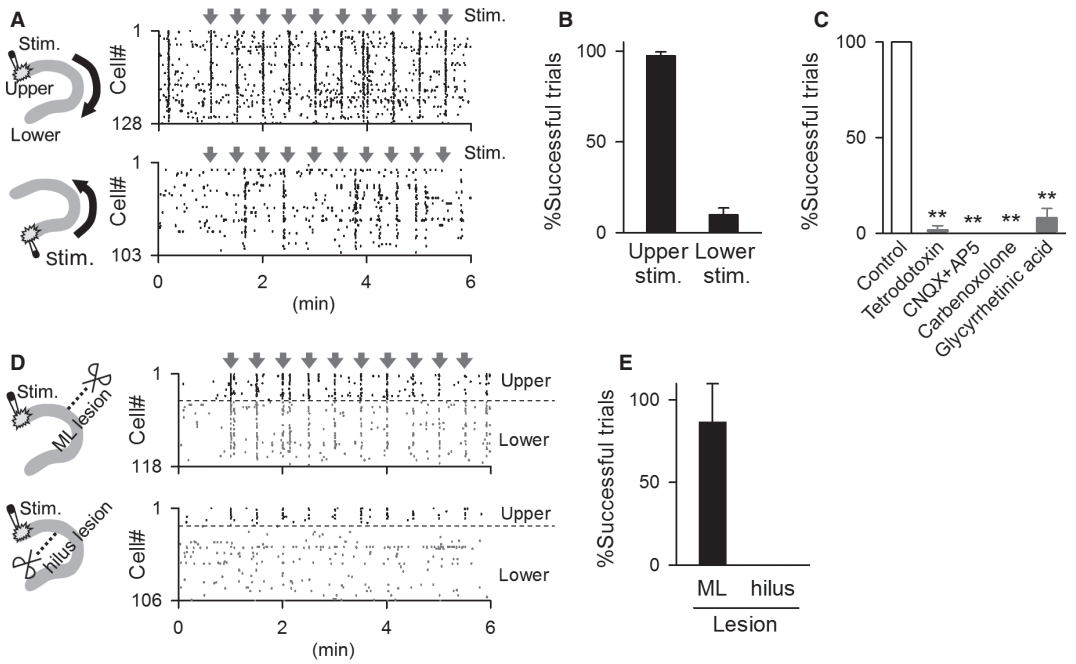

FIG. 5. Electrical stimulation initiates unidirectional traveling waves in immature DG networks. (A) Waves were elicited by electrical stimulation (three 30-μA pulses at 100 Hz) to the tip of the upper blade (top) but not the lower blade (bottom) of the DG granule cell layer in P3 slices. Arrows indicate the timing of stimulation. (B) Data are from five slices from three animals for each group. The ordinate indicates the probability that a stimulus evoked a wave. (C) Pharmacological characterization of stimulation-evoked waves. n = 5–6 slices from three to four animals each; $^{**}P < 0.01$ vs. control; Dunnett's test after one-way ANOVA. (D) Electrical stimulation was applied to the upper blade tip in P3 slices in which the molecular layer (ML) (top) or the hilus (bottom) was transversely incised using a mini-scalpel. Waves did not traverse the incised hilus. (E) Data are from three to four slices of two animals each. Error bars represent SEMs. AP5, D,L-2-amino-5-phosphonopentanoic acid; CNQX, 6-cyano-7-nitroquinoxaline-2,3-dione.

transmission is more pivotal in wave propagation than electrical synapses.

The circuit mechanism cannot be fully deduced by the present work alone; however, several possibilities can be imagined based on the data of our pharmacological and surgical experiments. First, DG waves required the activity of electric synapses. In DG granule cells, gap junctions exist on their mossy fiber axons and electrically couple these axons in the stratum lucidum of the CA3 field close to the DG (Hamzei-Sichani *et al.*, 2007). Therefore, it is plausible that the axo-axon coupling mediates the DG wave propagation. Second, DG waves required the activity of glutamate receptors. Glutamate receptors usually exist on postsynaptic dendrites. Considering that surgical lesion of the hilus, but not the molecular layer, prevented DG waves, one possible mechanism underlying the wave propagation is that, early in development, the axons of granule cells may project to proximal dendrites of neighboring granule cells and sequentially activate downstream neurons (Supporting Information Fig. S2A), although the anatomical evidence is lacking. The second possibility is inspired by the fact that immature granule cells express functional glutamate receptors on their axons (Tashiro *et al.*, 2003). Thus, glutamate released from synaptic terminals may activate axonal glutamate receptors and transmits the wave activity to downstream neurons (Supporting Information Fig. S2B). Finally, the wave propagation may be mediated by hilar mossy cells, which are known to receive direct inputs from granule cells and project to proximal dendrites of granule cells (Supporting Information Fig. S2C).

It should be noted that the circuit mechanism for waves in other regions has been shown to shift dramatically during development (Blankenship & Feller, 2010). Multiple mechanisms may operate in DG waves. Moreover, the immature hippocampus exhibits different types of early network oscillations, including synchronous plateau assemblies (Crepel *et al.*, 2007; Allene *et al.*, 2008) and giant depolarizing potentials (Ben-Ari *et al.*, 1989; Leinekugel *et al.*, 1997). These oscillations may crosstalk with the DG wave and influence the wave mechanisms.

Function of dentate gyrus waves

Although early network oscillations in the hippocampus and neocortex are believed to shape neuronal development, to date there is no definitive evidence of a causal link. This lack of evidence is, at least in part, due to a lack of experimental procedures that can specifically manipulate the generation or frequency of network waves. Therefore, our finding that DG waves were prevented by prenatal stress is important for the understanding of the function of the waves because the malformation of dendrites in DG granule cells appeared thereafter. Moreover, to our knowledge, our work is the first to demonstrate the stress sensitivity of early network waves.

It is intriguing that the DG slices of stressed mice were capable of generating waves in response to electrical stimulation. The speed and direction of the evoked waves were similar to those of spontaneously occurring waves in control mice, which suggests that, even in stressed mice, the network basis that supports the DG wave propagation was intact. Consistent with this result, we found no dendritic aberration in the DGs of stressed P3 mice, although the electrophysiological intrinsic properties were altered. Care must be taken to interpret the altered intrinsic properties, because one cannot determine whether they resulted in or from the DG wave deficits. The decreased membrane capacitance and the increased membrane resistance of DG granule cells seemed to reflect a retarded maturation of neuronal physiology. Electrophysiologically, they must lead to an increase in the sensitivity of their membrane

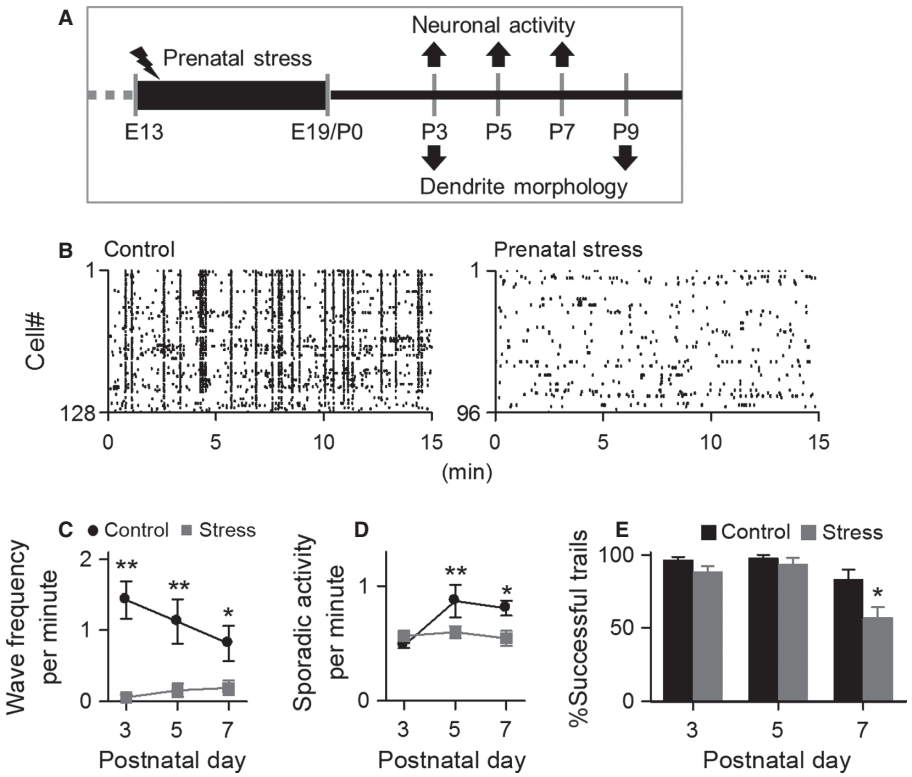

FIG. 6. Prenatal stress prevents spontaneous (but not evoked) DG waves. (A) Experimental schedules. Embryonic day (E)13–19 pregnant mice were exposed daily to restraint stress. (B) Representative activity patterns of P3 DG in control mice (left) and mice that experienced prenatal stress (right). Developmental changes in the frequency of traveling waves (C) and sporadic activity (D) in P3, P5, and P7 mice that did or did not experience prenatal stress. n = 5–6 slices from three to four animals for each group. (E) Probability that an electrical stimulus to the DG upper blade tip evoked a wave event. n = 5–7 slices from three to four animals each; $^*P < 0.05$, $^{**}P < 0.01$ vs. control, Tukey multiple comparison test after two-way ANOVA. Error bars represent SEMs.

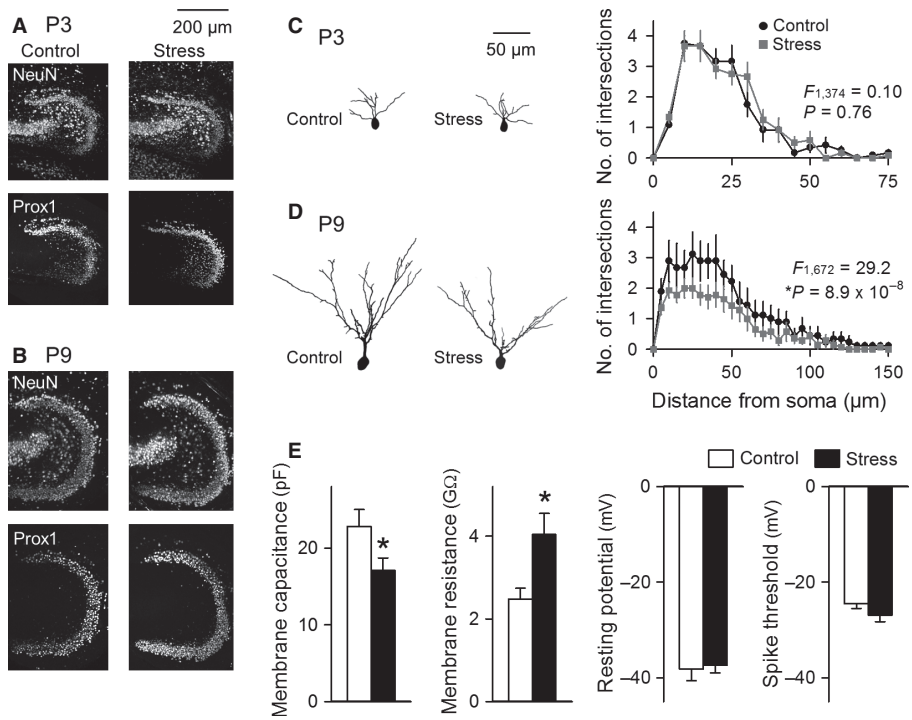

FIG. 7. Prenatal stress causes dendritic atrophy. Confocal images of DG immunostained against neuronal nuclear antigen and Prox1 in control mice (control) and mice that experienced prenatal stress (stress) at P3 (A) and P9 (B). The morphologies of dendrites of DG granule cells in control mice (control) and mice that experienced prenatal stress (stress) were analyzed at P3 (C) and P9 (D). Representative somatodendritic morphology of granule cells (left) and the Sholl analysis of dendrites of granule cells (right). n = 9–14 cells from 5 to 11 slices of four animals each, two-way repeated-measures ANOVA. The F and P values for the main effect are shown in each panel. Error bars represent SEMs. (E) The membrane capacitance, membrane resistance, resting membrane potential, and action potential threshold were recorded from P3 to P4 slices using whole-cell patch-clamp recording. n = 12–15 cells of 10 slices from three to four animals each. $^*P < 0.05$, Student's t-test. Error bars represent SEMs.

potentials to synaptic inputs. Nonetheless, the wave disappeared after prenatal stress. Therefore, the observed change in the intrinsic membrane properties may reflect a homeostatic compensation for stress-induced decreases in network activity. Taken together, the neuronal system sensitivity to prenatal stress is not attributable to the changed excitability of individual neurons, but rather it is more likely to result from the deficit of an initiator (or pace maker) of DG waves, which probably exists within the tip of the upper blade of the granule cell layer. Influential 'hub' neurons are reported to be capable of initiating global network oscillations in the immature hippocampus (Bonifazi *et al.*, 2009; Picardo *et al.*, 2011). A similar initiator may exist in immature DG networks and be vulnerable to stress.

Significant downregulations of hippocampal genes, including presynaptic voltage-gated calcium and potassium channels, are reported in 23-day-old female offspring of rats stressed during gestation (Bogoch *et al.*, 2007), but it should be noted that a DG wave deficit is one of the earliest pathological manifestations previously reported in the prenatally stressed brain. Therefore, the wave deficit may constitute a core of the long-term effect of prenatal stress. In this respect, it is intriguing to see our recent findings that mineralocorticoid receptors are downregulated in granule cells in prenatally stressed rats at later postnatal ages and that pharmacological activation of mineralocorticoid receptors rescues stress-induced impairment of granule cell maturation (Tamura *et al.*, 2011). Further studies are required to evaluate the causal effect of the wave deficit on mineralocorticoid receptor downregulation and dendritic atrophy. In addition, our previous study indicates that male pups are more susceptible to prenatal stress compared with female pups in terms of dendritic atrophy. Although we did not discriminate the sex of offspring in the present work, the sex difference in wave generation is an interesting topic for future studies.

Perinatal stress is widely known to cause long-lasting malfunctioning of the brain, such as cognitive and emotional problems, that often persists throughout the life span of the offspring (Heim & Nemeroff, 2002; McEwen, 2003; Weinstock, 2008). The hippocampus, in particular, is susceptible to stress and exhibits a reduced volume in depressive patients (Sheline *et al.*, 1996; Bremner *et al.*, 2000). A reduction in hippocampal volume is also observed in patients who suffer from early childhood trauma (Vythilingam *et al.*, 2002). Therefore, abnormal structure and function of the hippocampus following early life stress are putative risk factors for stress-related disorders in adults. In animal models, we found that the dendritic atrophy of DG neurons was observed in P9 but not P3 mice and was preceded by a lack of DG waves. Thus, the wave deficit could be a therapeutic target for the possible aversive sequelae of perinatal stress.

Supporting Information

Additional supporting information can be found in the online version of this article:

Fig. S1. No effect of the temperature of perfusion solution on calcium activities.

Fig. S2. Three possible circuit mechanisms of wave propagation.

Please note: As a service to our authors and readers, this journal provides supporting information supplied by the authors. Such materials are peer-reviewed and may be re-organized for online delivery, but are not copy-edited or typeset by Wiley-Blackwell. Technical support issues arising from supporting information (other than missing files) should be addressed to the authors.

Acknowledgements

This work was supported in part by Grants-in-Aid for Science Research (nos. 18021008, 22115003, 22390012, 22650080 and 22680025) from the Ministry of Education, Culture, Sports, Science and Technology of Japan, the Suzuken Memorial Foundation, the Kanae Foundation for the Promotion of Medical Science, the Daiichi-Sankyo Foundation of Life Science, and the Funding Program for Next Generation World-Leading Researchers (no. LS023).

Abbreviations

aCSF, artificial cerebrospinal fluid; DG, dentate gyrus; P, postnatal day.

References

Afadlal, S., Polaboon, N., Surakul, P., Govitrapong, P. & Jutapakdeegul, N. (2010) Prenatal stress alters presynaptic marker proteins in the hippocampus of rat pups. *Neurosci. Lett.*, **470**, 24–27.

Aleksandrov, A.A., Polyakova, O.N. & Batuev, A.S. (2001) The effects of prenatal stress on learning in rats in a Morris maze. *Neurosci. Behav. Physiol.*, **31**, 71–74.

Allene, C., Cattani, A., Ackman, J.B., Bonifazi, P., Aniksztejn, L., Ben-Ari, Y. & Cossart, R. (2008) Sequential generation of two distinct synapse-driven network patterns in developing neocortex. *J. Neurosci.*, **28**, 12851–12863.

Altman, J. & Bayer, S.A. (1990) Migration and distribution of two populations of hippocampal granule cell precursors during the perinatal and postnatal periods. *J. Comp. Neurol.*, **301**, 365–381.

Ben-Ari, Y., Cherubini, E., Corradetti, R. & Gaiarsa, J.L. (1989) Giant synaptic potentials in immature rat CA3 hippocampal neurones. *J. Physiol.*, **416**, 303–325.

Blankenship, A.G. & Feller, M.B. (2010) Mechanisms underlying spontaneous patterned activity in developing neural circuits. *Nat. Rev. Neurosci.*, **11**, 18–29.

Bogoch, Y., Biala, Y.N., Linial, M. & Weinstock, M. (2007) Anxiety induced by prenatal stress is associated with suppression of hippocampal genes involved in synaptic function. *J. Neurochem.*, **101**, 1018–1030.

Bonifazi, P., Goldin, M., Picardo, M.A., Jorquera, I., Cattani, A., Bianconi, G., Represa, A., Ben-Ari, Y. & Cossart, R. (2009) GABAergic hub neurons orchestrate synchrony in developing hippocampal networks. *Science*, **326**, 1419–1424.

Bremner, J.D., Narayan, M., Anderson, E.R., Staib, L.H., Miller, H.L. & Charney, D.S. (2000) Hippocampal volume reduction in major depression. *Am. J. Psychiatry*, **157**, 115–118.

Claiborne, B.J., Amaral, D.G. & Cowan, W.M. (1990) Quantitative, three-dimensional analysis of granule cell dendrites in the rat dentate gyrus. *J. Comp. Neurol.*, **302**, 206–219.

Crepel, V., Aronov, D., Jorquera, I., Represa, A., Ben-Ari, Y. & Cossart, R. (2007) A parturition-associated nonsynaptic coherent activity pattern in the developing hippocampus. *Neuron*, **54**, 105–120.

Garaschuk, O., Linn, J., Eilers, J. & Konnerth, A. (2000) Large-scale oscillatory calcium waves in the immature cortex. *Nat. Neurosci.*, **3**, 452–459.

Hamzei-Sichani, F., Kamasawa, N., Janssen, W.G., Yasumura, T., Davidson, K.G., Hof, P.R., Wearne, S.L., Stewart, M.G., Young, S.R., Whittington, M.A., Rash, J.E. & Traub, R.D. (2007) Gap junctions on hippocampal mossy fiber axons demonstrated by thin-section electron microscopy and freeze fracture replica immunogold labeling. *Proc. Natl. Acad. Sci. USA*, **104**, 12548–12553.

Heim, C. & Nemeroff, C.B. (2002) Neurobiology of early life stress: clinical studies. *Semin. Clin. Neuropsychiatry*, **7**, 147–159.

Hosseini-Sharifabad, M. & Hadinedoushan, H. (2007) Prenatal stress induces learning deficits and is associated with a decrease in granules and CA3 cell dendritic tree size in rat hippocampus. *Anat. Sci. Int.*, **82**, 211–217.

Leinekugel, X., Medina, I., Khalilov, I., Ben-Ari, Y. & Khazipov, R. (1997) Ca^{2+} oscillations mediated by the synergistic excitatory actions of $GABA_A$ and NMDA receptors in the neonatal hippocampus. *Neuron*, **18**, 243–255.

Lemaire, V., Koehl, M., Le Moal, M. & Abrous, D.N. (2000) Prenatal stress produces learning deficits associated with an inhibition of neurogenesis in the hippocampus. *Proc. Natl. Acad. Sci. USA*, **97**, 11032–11037.

Martinez-Tellez, R.I., Hernandez-Torres, E., Gamboa, C. & Flores, G. (2009) Prenatal stress alters spine density and dendritic length of nucleus accumbens and hippocampus neurons in rat offspring. *Synapse*, **63**, 794–804.

McEwen, B.S. (2003) Early life influences on life-long patterns of behavior and health. *Ment. Retard. Dev. Disabil. Res. Rev.*, **9**, 149–154.
McLaughlin, T., Torborg, C.L., Feller, M.B. & O'Leary, D.D. (2003) Retinotopic map refinement requires spontaneous retinal waves during a brief critical period of development. *Neuron*, **40**, 1147–1160.
Muramatsu, R., Ikegaya, Y., Matsuki, N. & Koyama, R. (2007) Neonatally born granule cells numerically dominate adult mice dentate gyrus. *Neuroscience*, **148**, 593–598.
Picardo, M.A., Guigue, P., Bonifazi, P., Batista-Brito, R., Allene, C., Ribas, A., Fishell, G., Baude, A. & Cossart, R. (2011) Pioneer GABA cells comprise a subpopulation of hub neurons in the developing hippocampus. *Neuron*, **71**, 695–709.
Sasaki, T., Matsuki, N. & Ikegaya, Y. (2007) Metastability of active CA3 networks. *J. Neurosci.*, **27**, 517–528.
Sasaki, T., Matsuki, N. & Ikegaya, Y. (2011) Action-potential modulation during axonal conduction. *Science*, **311**, 599–601.
Seay-Lowe, S.L. & Claiborne, B.J. (1992) Morphology of intracellularly labeled interneurons in the dentate gyrus of the immature rat. *J. Comp. Neurol.*, **324**, 23–36.
Sheline, Y.I., Wang, P.W., Gado, M.H., Csernansky, J.G. & Vannier, M.W. (1996) Hippocampal atrophy in recurrent major depression. *Proc. Natl. Acad. Sci. USA*, **93**, 3908–3913.
Spitzer, N.C. (2006) Electrical activity in early neuronal development. *Nature*, **444**, 707–712.
Takahashi, N., Kitamura, K., Matsuo, N., Mayford, M., Kano, M., Matsuki, N. & Ikegaya, Y. (2012) Locally synchronized synaptic inputs. *Science*, **335**, 353–356.
Tamura, M., Sajo, M., Kakita, A., Matsuki, N. & Koyama, R. (2011) Prenatal stress inhibits neuronal maturation through downregulation of mineralocorticoid receptors. *J. Neurosci.*, **31**, 11505–11514.
Tashiro, A., Dunaevsky, A., Blazeski, R., Mason, C.A. & Yuste, R. (2003) Bidirectional regulation of hippocampal mossy fiber filopodial motility by kainate receptors: a two-step model of synaptogenesis. *Neuron*, **38**, 773–784.
Tritsch, N.X., Yi, E., Gale, J.E., Glowatzki, E. & Bergles, D.E. (2007) The origin of spontaneous activity in the developing auditory system. *Nature*, **450**, 50–55.
Vythilingam, M., Heim, C., Newport, J., Miller, A.H., Anderson, E., Bronen, R., Brummer, M., Staib, L., Vermetten, E., Charney, D.S., Nemeroff, C.B. & Bremner, J.D. (2002) Childhood trauma associated with smaller hippocampal volume in women with major depression. *Am. J. Psychiatry*, **159**, 2072–2080.
Watt, A.J., Cuntz, H., Mori, M., Nusser, Z., Sjostrom, P.J. & Hausser, M. (2009) Traveling waves in developing cerebellar cortex mediated by asymmetrical Purkinje cell connectivity. *Nat. Neurosci.*, **12**, 463–473.
Weinstock, M. (2008) The long-term behavioural consequences of prenatal stress. *Neurosci. Biobehav. Rev.*, **32**, 1073–1086.
Yuste, R., Peinado, A. & Katz, L.C. (1992) Neuronal domains in developing neocortex. *Science*, **257**, 665–669.